BIOCHEMISTRY
including biophysical chemistry & molecular biology

Article

pubs.acs.org/biochemistry

Stem-Forming Regions That Are Essential for the Amyloidogenesis of Prion Proteins

Masatoshi Saiki,[†,‡,§,⊥] Yuji Hidaka,[†] Masayuki Nara,[∥] and Hisayuki Morii*[,‡]

[†]School of Science and Engineering, Kinki University, Kowakae, Higashi-Osaka, Osaka 577-8502, Japan
[‡]National Institute of Advanced Industrial Science and Technology (AIST), Central 6, Tsukuba, Ibaraki 305-8566, Japan
[§]Faculty of Engineering, Tokyo University of Science, Yamaguchi, Sanyo-Onoda, Yamaguchi 756-0884, Japan
[∥]Laboratory of Chemistry, Tokyo Medical and Dental University, Ichikawa, Chiba 272-0827, Japan

Supporting Information

ABSTRACT: Prion diseases represent fatal neurodegenerative disorders caused by the aggregation of prion proteins. With regard to the formation of the amyloidogenic cross-β-structure, the initial mechanism in the conversion to a β-structure is critically important. To explore the core regions forming a stem of the amyloid, we designed and prepared a series of peptides comprised of two native sequences linked by a turn-inducing dipeptide moiety and examined their ability to produce amyloids. A sequence alignment of the peptides bearing the ability to form amyloid structures revealed that paired strands consisting of VNITI (residues 180−184) and VTTTT (residues 189−193) are the core regions responsible for initiating the formation of cross-β-structures and for further ordered aggregation. In addition, most of the causative mutations responsible for inherited prion diseases were found to be located in these stem-forming regions on helix H2 and their counterpart on helix H3. Moreover, the volume effect of the nonstem domain, which contains ∼200 residues, was deduced to be a determinant of the nature of the association such as oligomerization, because the stem-forming domain is only a small part of a prion protein. Taken together, we conclude that the mechanism underlying the initial stage of amyloidogenesis is the exposure of a newly formed intramolecular β-sheet to a solvent through the partial transition of a native structure from an α-helix to a β-structure. Our results also demonstrate that prion diseases caused by major prion proteins except the prions of some fungi such as yeast are inherent only in mammals, as evidenced by a comparison of the corresponding sequences to the stem-forming regions among different animals.

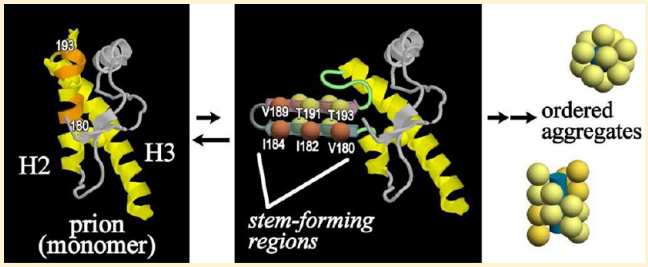

The aggregation of prion protein (PrP) is responsible for a number of fatal neurodegenerative diseases known as prion diseases, including bovine spongiform encephalopathy and Creutzfeldt-Jakob disease (CJD). Normal prion protein exists in a relatively α-helix-rich form and is harmless.[1,2] In contrast, pathogenic prion proteins are rodlike particles 10−20 nm in diameter. These aggregates show birefringence in the presence of Congo red, suggesting amyloid-like molecular integration,[3] which mainly involves β-structures that are different from the secondary structure of a monomer.[4] Scrapie prion protein (PrP^{Sc}) shows the highest infectivity in particles 17−27 nm in diameter.[5] This indicates that the aggregation with a specific size is essential for the pathogenicity and infectivity of prions. Nevertheless, the issue of specifically how normal PrP [cellular prion protein (PrP^{C})] undergoes transformation into an aggregated form remains unclear. As a result, a better understanding of the mechanism for this transformation, at the molecular level, is an important issue, in terms of our understanding of prion diseases.

Aggregated PrP(27−30), which is produced by treating PrP^{Sc} with proteinase K, retains its infectivity even though it lacks ∼90 N-terminal residues.[6] This proves that both the pathogenicity and the infectivity of this prion protein originate in the region of residues 90−230. In addition, recombinant PrP with a full-length amino acid chain was found to form amyloids and oligomers,[7] indicating that amyloid formation is clearly derived from the nature of the peptide chain itself. It was recently reported that a sheep PrP(167−227) fragment, which corresponds to two major α-helix regions (H2 and H3) in PrP, formed an amyloid structure similar to that of full-length PrP.[8] Thus, the essential information for amyloid formation is likely to be located in the H2−H3 region. On the other hand, the injection of amyloid-formed P101L-PrP(89−143) is known to cause Gerstmann-Straussler disease (GSD) for the mouse,[9] suggesting the existence of another site that is essential for amyloid formation. Various causative mutations have been discovered in both regions. Interestingly, the pathogenic mutations in the former region (residues 167−227) involve

Received: November 10, 2011
Revised: February 4, 2012
Published: February 10, 2012

mostly CJD, and those in the latter (residues 89−143) have relevance in GSD.

Among the various prion fragments examined, amyloid formation was detected for peptides 109−122, 113−127, 178−191, and 202−218 of Syrian hamster PrP[10] and for peptides 106−126 and 127−147 of human PrP.[11] Via analysis of proteinase K-resistant regions, peptide 122−221 for PrP(89−231) and peptides 134−140 and 177−217 for PrP106, which is a construct with a combined sequence of residues 89−140 and 177−231, were found to be protected from proteolysis because of β-structure formation.[12] In summary, it appears that the regions relevant to the formation of an amyloid-like β-structure are peptides 109−143 and 178−218. However, the core region responsible for the formation of a cross-β-structure has not been unequivocally identified, because amyloid formation of fragment peptides is not always compatible with the structural change in the corresponding region in a full-length protein.

The aggregation to amyloid fibrils from PrP or recombinant PrP(90−231) can be achieved by converting the solvent from an aqueous solution of 0.2% sodium dodecyl sulfate (SDS) to a buffer solution with a neutral pH.[13] In the course of this transition, a dimer and oligomers of PrP's are also formed. The dimer exists in equilibrium with the monomers, with a locally transformed structure recognized as a soluble fibril precursor state.[14] The activation energy for the transition from dimer to oligomer of PrP's is relatively high, and the transition to aggregated PrP^{Sc} is deduced to be linked to the exposure of a hydrophobic moiety.[15] The precursor for the oligomers, which is generated by refolding PrP through a detergent-denatured state, has molten globule characteristics.[16] The oligomers are reportedly octamers[12] or almost decamers.[16,17] These findings imply that the formation of fibrils is a relatively difficult event in contrast with the formation of amyloids from short peptides.

As for the structure of PrP in amyloids, H−D exchange mass spectroscopy[18,19] has been applied as well as electron paramagnetic resonance spectroscopy for a spin-labeled Cys mutant PrP.[20] The results revealed that a region such as peptide 163−223, nearly the same as the region corresponding to H2 and H3, is strongly shielded from the solvent. It therefore appears that this region contains core parts that are crucial for amyloid formation. Similarly, solid-state nuclear magnetic resonance (NMR) data with a Monte Carlo−simulated annealing algorithm suggest that the core is comprised of residues 173−224.[21] In addition, NMR analyses of the monomeric form of a soluble prion protein revealed that the region of H2 and H3 is structurally unstable.[22] Considering the information obtained so far, the core region responsible for amyloidogenesis is most likely located in peptide 170−220 and its vicinity. However, the precise assignment of respective amino acid residues for the secondary structures including a cross-β-structure continues to be an important issue. Here, we define the term "stem-forming region" for convenience, which denotes the region of the cross-β-structure with successive hydrogen bonds along with the fibril axis. This work was conducted in an attempt to identify the stem-forming region that plays an essential role in amyloid formation. The clarification of the precise structure of the stem-forming region would be important for understanding the dynamic behavior of PrP, such as molecular integration and conformational transition. It should also be useful in terms of elucidating the origin of pathogenicity and the development of detection methods.

We previously reported on fundamental rules for regulating the structural formation of amyloids by employing various mutations and designs for barnase fragments.[23] On the basis of this rule, which is based mainly on the hydrophobic interaction between side chains, a method that predicts the propensity for amyloidogenicity was developed.[24] The method strongly indicated that residues 170−220 of PrP are relevant to the stem-forming region. Moreover, the predictions were verified by a molecular design utilizing a turn-inducing sequence with a D-amino acid residue.[24,25] In the work presented here, the design of a turn-inducing sequence was effectively used to search for the stem-forming region. Here, via rational interpretation of the experimental data, we propose the stem-forming region of PrP with a high degree of reliability for the first time.

MATERIALS AND METHODS

Synthesis of Peptides with Native and Designed Sequences. The peptides were prepared by the Fmoc solid-phase method using Fmoc-NH-SAL-PEG resin (Watanabe Chemicals) for the peptide chains with C-terminal amide groups.[26] Chain elongation was performed with Fmoc amino acids and activation reagents 2-(1*H*-benzotriazol-1-yl)-1,1,3,3-tetramethyluronium hexafluorophosphate, 1-hydroxybenzotriazole, and *N*-methylmorpholine (1:1:2 molar ratio). To remove the Fmoc group, an *N*,*N*-dimethylformamide (DMF) solution containing 1,8-diazabicyclo[5.4.0]-7-undecene, piperidine, and 1-hydroxybenzotriazole (1.2%, 8%, and 2.5%, respectively) was employed. The final cleavage reaction was conducted with trifluoroacetic acid, 1,2-ethanedithiol, triisopropylsilane, and water (86:6:6:2 volume ratio). The peptides obtained by precipitation with diethyl ether were purified by reverse-phase high-performance liquid chromatography (HPLC) and identified by electrospray ionization mass spectometry (Shimadzu QP-8000α spectrometer).

For the peptides that were produced in low yields by the usual method as described above, the esterification reaction to the hydroxyl group of threonine was incorporated as an alternative to the general coupling reaction.[27] For example, peptide Prf09 was successfully synthesized through esterification at Thr183 and Thr192. Prior to esterification, the Boc-protected threonine was coupled to a peptide chain with diisopropylcarbodiimide (DIC) and 1-hydroxybenzotriazole. Esterification for the hydroxyl group of the threonine residue was performed with Fmoc amino acid (0.3 M) and DIC (1 equiv) in the presence of 4-(*N*,*N*-dimethylamino)pyridine (0.06 equiv) for 45 min in a CH_2Cl_2/DMF solvent. Following HPLC purification, the rearrangement from the ester linkage to the desired amide linkage was conducted in a sodium acetate buffer (pH 7.4) solution containing 20 mM dithiothreitol (DTT) for 5 h.

To prevent the risk of pathogenic synthetic peptides, non-natural D-amino acids were employed, except for L-alanine in a turn-inducing sequence, (D-Asp)-(L-Ala). This could be reasonably warranted by the lack of cross-reactivity between the L-peptide and D-peptide in amyloid formation.[28]

Amyloid Formation. The stock solution containing 40 nmol of synthetic peptide was first dried in a vacuum, and the peptide was then dissolved in DMF (8 μL) containing 4% LiCl, which typically is effective for assuring a solubilized state. Amyloid formation was initiated by diluting the solution described above with 50 mM buffer solution (192 μL) containing Na_2HPO_4/citric acid (pH 4.5 and 5.5), Na_2HPO_4/

dx.doi.org/10.1021/bi201688r | *Biochemistry* 2012, 51, 1566−1576

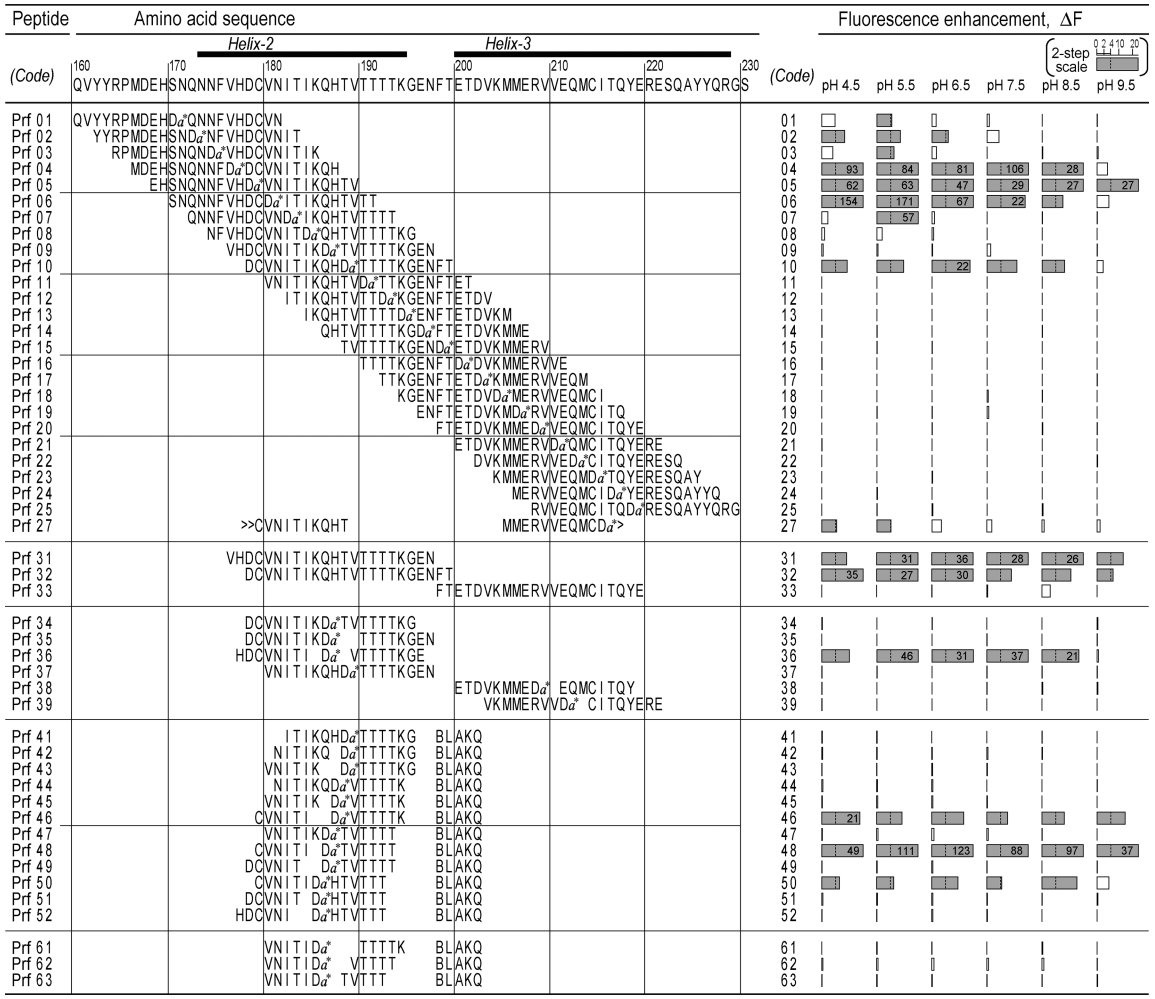

Figure 1. Amino acid sequences of the synthetic peptides and the results of a ThT binding assay to detect amyloidogenicity. All peptides were coded as "Prf" with a sequential number. The native sequence of human prion protein is indicated in the first row. The chirality of the residues is generally of the D type. In the sequence, *a** and B denote L-Ala and *β*-Ala, respectively. The special sequences, D*a** and BLAKQ, are designed for turn inducing and adequate solubility, respectively. The sequence of Prf27 is MMERVVEQMC-D*a**-CVNITIKQHT. The fluorescence enhancement, Δ*F*, of an incubated peptide solution is shown in the same row as the corresponding sequence. The values of Δ*F* as a measure of amyloidogenicity are shown with bar graphs, of which the scale is given in a two-step manner switched at the value of 4 in order to zoom up the lower values. The upper limit of the graph was fixed at 25. Δ*F* values of >20 are indicated with numerical values.

NaH_2PO_4 (pH 6.5), Tris-HCl (pH 7.5), or $Na_2B_4O_7$-HCl/NaOH (pH 8.5 and 9.5). The incubation was pursued for generally 2 days at a peptide concentration of 0.2 mM in the presence of 4 mM DTT for Cys-containing peptides under static conditions at 4 °C.

Thioflavin T Binding Assay. Amyloid formation was evaluated by the fluorescence enhancement of amyloid-bound thioflavin T (ThT). An aliquot was sampled from the incubation solution and diluted 100-fold with potassium phosphate buffer (pH 7.0) containing 5 μM ThT. Fluorescence spectra of the samples in polystyrene cuvettes were recorded at wavelengths of 460−600 nm (bandwidth, 5 nm) by excitation at 450 nm (bandwidth, 5 nm) at 20 °C with a Hitachi F2500 fluorescence spectrometer. The bands derived from Raman scattering were compensated computationally. Fluorescence enhancement of ThT in the amyloid-bound state, Δ*F*, was defined as $\Delta F = (F_S - F_0)/F_0$, where F_S and F_0 denote the fluorescence intensity of a sample and that of a control solution without peptides, respectively.

Electron Microscopy. The sample solution containing amyloids, as detected by the ThT binding assay, was placed on a collodion-coated copper grid and then rinsed with 1% (w/v) aqueous uranyl acetate to create a negative stain. After the sample grid had been dried, vaporized carbon was deposited on the sample under a vacuum. The fibrils were photographed with a transmission electron microscope (Hitachi model H-7000) at 75 kV.

Circular Dichroism Spectroscopy. Circular dichroism (CD) spectra were recorded in the far-UV region (190−260 nm) at 20 °C with a JASCO J-805 spectropolarimeter using a quartz cuvette with a 0.2 mm path length. The spectral data were recorded in terms of mean residue ellipticity, [*θ*], in degrees square centimeter per decimole. Noise from the spectra was reduced by approximating the raw data with the linear combination of Gaussian curves.

IR Spectroscopy. A stock solution containing the peptide (140 nmol) was dried in a vacuum in the presence of DTT (2 μmol). The peptide was dissolved with a 4% LiCl/DMF mixture and diluted with D_2O to exchange dissociable hydrogen atoms in the peptide with deuterium. This peptide solution was evaporated to dryness. The resulting peptide was subjected to incubation for amyloid formation as described

dx.doi.org/10.1021/bi201688r | *Biochemistry* 2012, 51, 1566−1576

above in a deuterated buffer solution. The peptide, in the form of amyloids, was collected by centrifugation and then washed twice with D_2O (700 μL). The collected amyloids were analyzed by infrared (IR) spectroscopy using the attenuated total reflection (ATR) method at the interface between a diamond plate and the sample.[29] The measurement was taken with a Perkin-Elmer Spectrum One FT-IR apparatus using a mercury cadmium telluride (MCT) detector cooled by liquid nitrogen. The raw data were refined by subtracting the signal of vaporized water and normalized at the highest peak around 1620 cm^{-1} with reference to the value at 1727 cm^{-1}. To clarify the secondary structures of the amyloids, we resolved the spectra into Gaussian curves with ~30 cm^{-1} bandwidth, with the peak positions selected as around 1680−1678, 1658−1653, 1634−1642, and 1622−1614 cm^{-1}. It is noteworthy that for the absorption band for the β-structure around 1619−1613 cm^{-1}, an additional sharp Gaussian curve with a 10−15 cm^{-1} bandwidth was combined with the ordinary one at 1622−1614 cm^{-1}.

RESULTS

Screening of Amyloid-Forming Peptides by ThT Binding. The stem-forming regions with cross-β-structures in amyloids were explored using synthetic peptides containing the parts of the native sequence that semiexhaustively covered the region of PrP(160−229), accompanied by a designed one. The sequence regions and the compositions of the peptides are denoted at the left side of Figure 1. The designed part consists of the Asp-Ala* sequence, where Ala* denotes a stereochemically inverse amino acid against most of the surrounding residues. Actually, (D-Asp)-(L-Ala) was inserted to link two different native sequences. It should be noted that the majority of the amino acid residues in the peptides of this work are non-natural D-type enantiomers to prevent biological hazards. The incorporation of Ala* effectively enhances the propensity to form a type II turn structure[30] in addition to breaking the continuity of the regular secondary structures. This approach offers the remarkable advantage of allowing us to search for the regions forming intramolecular β-sheet structures.[24] The systematic search was performed in two stages. The first was a study using (10 residues)-Asp-Ala*-(10 residues) peptides, e.g., (160−169)-Asp-Ala*-(172−181) (Prf01), as a specialized analogue for peptide 160−181.

The results of the ThT binding assay to examine amyloid forming properties are shown in Figure 1 (see Table S1 of the Supporting Information for the detailed values). On the basis of a previous report,[25] systems showing a fluorescence intensity, ΔF, of >8 were judged as participating in a significant amount of amyloid formation and those with ΔF values from 2 to 8 were judged as showing moderate formation. Cases in which the ΔF values were less than 0.32 were considered to produce no amyloid (see the details in Figures S1 and S2 of the Supporting Information). Peptides Prf04, Prf05, Prf06, and Prf10 exhibited significant amyloid forming properties over the wide range of pH values examined. Prf01, Prf02, Prf03, and Prf27 gave rise to amyloids to some extent, but only at acidic pH. Generally, amyloid formation that occurs only at acidic pH can be attributed to the participation of acidic residues such as Asp and Glu, so these latter peptides were excluded from the second stage of the search to obtain information under physiological conditions.

To narrow the search window, a series of peptides from Prf41 to Prf52 were designed as (6 residues)-Asp-Ala*-(6 residues)-(tail), where the tail region has a sequence of (β-Ala)-Leu-Ala-Lys-Gln to ensure relatively similar solubilities among the peptides.[24] The ThT binding properties of these are also indicated in Figure 1. Interestingly, amyloidogenicity was observed only for peptides such as Prf46, Prf48, and Prf50, probably because these peptides contain specific pairs of native sequences.

CD Spectra of Amyloids from Partially Designed Peptides. Representative CD spectra of the peptide solutions after incubation are shown in Figure 2. The peptides with no amyloidogenicity as revealed by ThT binding gave spectral patterns for random-coil structures with a positive band around 200 nm, of which the sign for ellipticity was derived from D-amino acid residues. Meanwhile, the peptides forming amyloids resulted in a CD spectral pattern with positive bands at 220−230 nm, which are specific to the cross-β-structure.[25] It should be noted that the signal intensity of Prf10 is ≥2 times greater than that of Prf04, Prf05, or Prf06. The spectrum of Prf32 with a fully native sequence bears a close resemblance to that of the semidesigned Prf10 covering the same region. In addition, Prf31 gave a CD spectrum similar to that of Prf32, though peptide Prf09 with a sequence corresponding to Prf31 shows only weak amyloid forming properties.

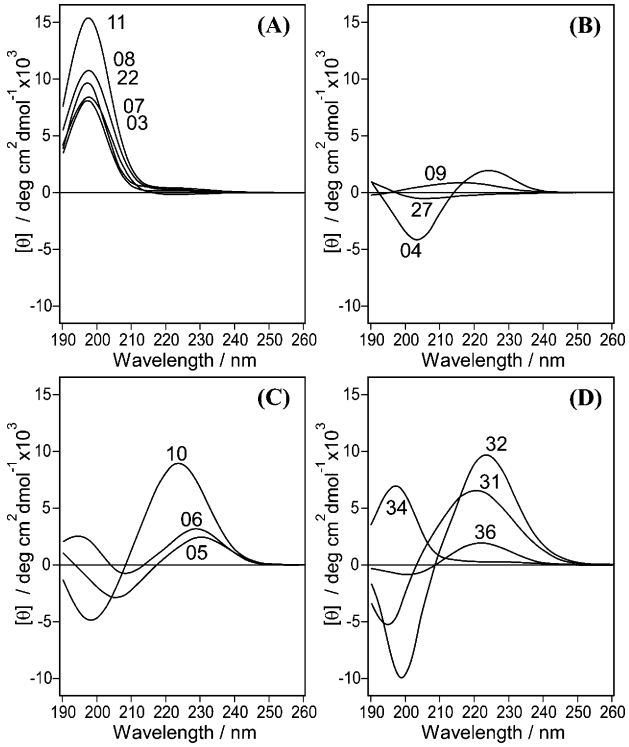

Figure 2. CD spectra of representative peptides after incubation for amyloid formation. The code numbers for the peptides, Prf, are indicated near the spectral curves. The CD spectra of Prf12−Prf25 were similar to those shown in panel A. It should be noted that the chirality of these peptides is basically a non-natural type, i.e., that of D-amino acid residues. Consequently, the signs of molar ellipticity ($[\theta]$) are opposite to those for general L-enantiomeric peptides at the respective bands. The spectra were smoothed by curve fitting with Gaussian curves. (A) CD spectra of the peptides showing random-coil structures. (B) and (C) CD spectra showing secondary structures other than random coils. (D) CD spectra of the peptides selected from Prf31−Prf39.

dx.doi.org/10.1021/bi201688r | Biochemistry 2012, 51, 1566−1576

IR Spectra of Amyloid Peptides. The IR spectra of most of the amyloid peptides exhibited a major band around 1620 cm^{-1} and a weaker band at 1680 cm^{-1}, indicating the formation of antiparallel β-structures (Figure 3 and Figure S3 of the Supporting Information).[31] This also indicates that these amyloids are likely to contain cross-β-structures.[32] In a comparison of Prf04 with Prf10, peptide Prf04 showed a relatively intense band at 1660−1640 cm^{-1} corresponding to a random-coil structure and a band for the β-structure weaker than that found for Prf10 (for the details, see Table S2 of the Supporting Information). This may be ascribed to a lower cross-β-structure content for Prf04. The spectrum of Prf10 resembles that of Prf31, covering the same region as Prf09, suggesting that peptides 176−197 and 178−199 have a common essential structure in amyloids. This is supported by the fact that the 18-residue peptide Prf36, which is composed of a pair of eight-residue peptides spanning the same region described above, showed a higher content of β-structure than Prf10 and Prf31 as 22-residue peptides.

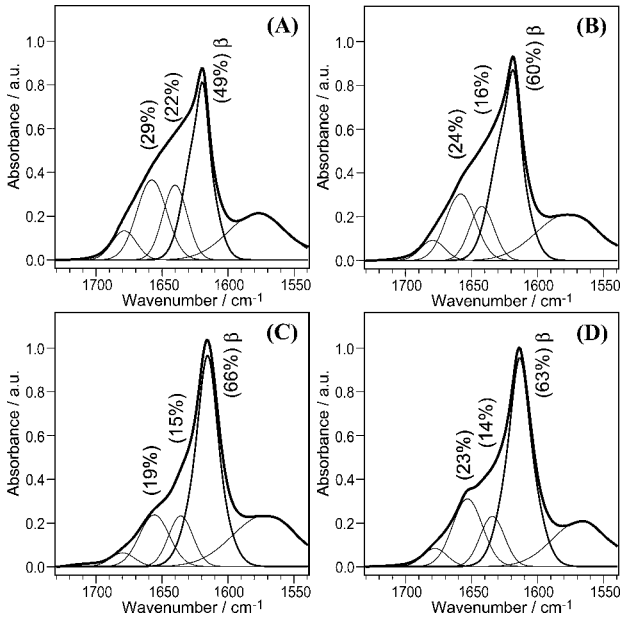

Figure 3. FT-IR spectra of amyloids obtained by incubation at pH 7.5. The exchangeable hydrogen atoms of the peptides are deuterated by using D_2O. The results for curve resolution are shown with Gaussian curves. The Gaussians numbered from the larger wavenumber, Gaussians 1−5, are assigned to parallel β-structure, random coils (some part being turns or bulges), random coils, β-structure, and amide II band, respectively (see Table S2 of the Supporting Information). The assignments of the respective bands are based on the reported values (see Table S2 of the Supporting Information). The signal around 1620 cm^{-1}, Gaussian 4, for β-structure is shown with combined Gaussians. Random coils are not uniquely assigned to a single Gaussian curve because of their diversity. The ratios of the areas for three representative bands, Gaussians 2−4, around 1650, 1635, and 1620 cm^{-1}, respectively, are shown in parentheses: (A) Prf04, (B) Prf10, (C) Prf36, and (D) Prf31.

Electron Microscopy Observation. Negatively stained images of the amyloids are shown in Figure 4. The amyloid fibrils of Prf04, Prf06, and Prf10 had ribbonlike structures, each bearing a striped-pattern texture with 4.0 nm intervals between the stripes (Figure 4E,F). Among these proteins, Prf04 appears to have a significant propensity to form irregular bundles of

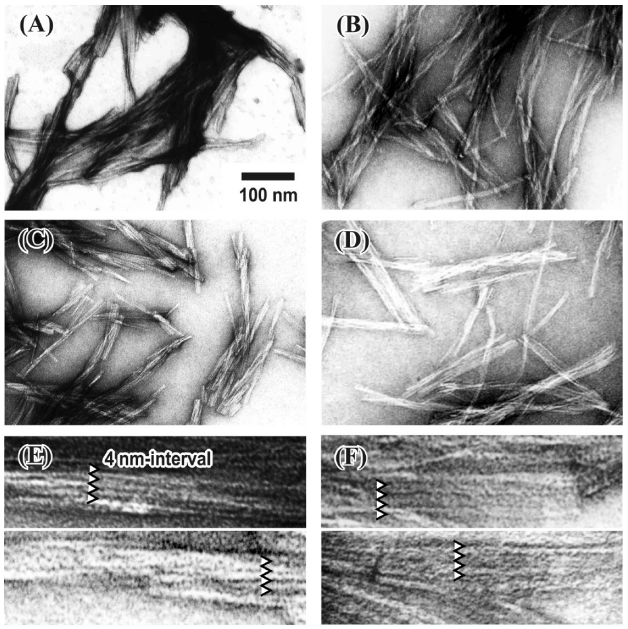

Figure 4. Electron microscopy photographs of the amyloids. The scale bar is the same for panels A−D. The amyloids are negatively stained. Enlarged photographs of panels C and D are shown in panels E and F, respectively, to exhibit the stripe patterns on the surface of the fibrils, where four triangle markers are aligned with every 4 nm interval: (A) Prf04, (B) Prf06, (C and E) Prf10, and (D and F) Prf32.

fibrils. Prf10 and Prf32, covering the same sequence (residues 178−199), exhibited an analogous morphology despite the difference in two residues in the middle region. Considering that two residues of Prf10, Asp-Ala* in the middle region, are incapable of forming a β-structure, Prf32 is likely to form a certain loop structure in the corresponding region. In other words, these two peptides may have a common composition of β-strands.

Fluorescence Spectra of ThT Bound to Amyloid. The binding of ThT molecules to the grooves of amyloid fibrils causes not only an enhancement of fluorescence intensity but also a blue shift in the maximal fluorescence wavelength.[25] In cases where the bound ThT is subject to a severe structural constraint, an extreme shift to a shorter wavelength is likely to occur. This leads to a larger fluorescence intensity ratio, F_P/F_{500}, where F_P and F_{500} denote the fluorescence intensities at the peak and at 500 nm, respectively. The system with an F_P/F_{500} value of >1.35 is indicative of a tight constraint for ThT in the grooves, as empirically suggested[25] (see Figure S2 of the Supporting Information for the details). The F_P/F_{500} values for the amyloids from Prf10, Prf31, and Prf36 were determined to be 1.48, 1.43, and 1.39, respectively, suggesting the formation of obvious grooves along the fibrils. Figure 5 shows fluorescence spectra of ThT-bound amyloid-forming peptides, each having a pair of six-residue native sequences. The F_P/F_{500} values for the amyloids from Prf46 and Prf48 were determined to be 1.52 and 1.49, respectively. These peptides have a common pair of sequences, VNITI and VTTTT. In contrast, the value for Prf50 was 1.14, probably because of a deficiency in the terminal Thr of VTTTT. Thus, the amyloid structure of Prf50 is clearly different from that of Prf46 or Prf48.

dx.doi.org/10.1021/bi201688r | Biochemistry 2012, 51, 1566−1576

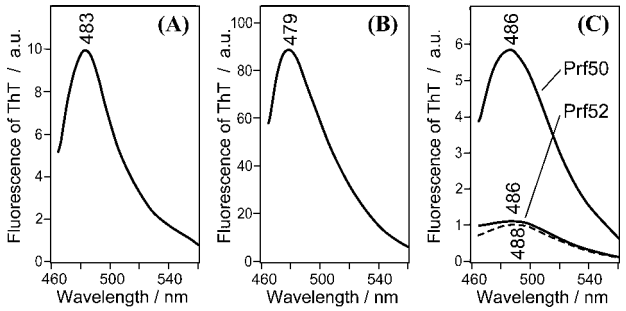

Figure 5. Fluorescence spectra of thioflavin T in the presence of the incubated peptides. The amyloids were prepared by incubation at pH 7.5. The control data without peptides are also shown with a dashed curve. The numbers at the peaks indicate maximal fluorescence wavelengths: (A) Prf46, (B) Prf48, and (C) Prf50 and Prf52 with a control.

DISCUSSION

Identification of Stem-Forming Regions. The first stage of the search for stem-forming regions was systematically conducted for the C-terminal sequence (residues 160−229), which involves the regions shielded against the solvent, because of the tight structure of the amyloids.[18,19] A remarkable amyloidogenicity was observed for Prf04−Prf06 and Prf10 over a wide pH range as well as at physiological pH. A highly hydrophobic sequence, VNITI, is present as peptide 180−184 in common for the sequences of Prf04, Prf05, and Prf10. On the other hand, Prf07 and Prf08, involving parts that are common with the peptides mentioned above, had rather low amyloidogenicities. This may be attributed to the fact that the designed Asp-Ala* sequence interferes in the region of residues 180−184 in the sequences of Prf07 and Prf08. This strongly suggests that the VNITI sequence plays a crucial role in amyloid formation.

Amyloid formation of Prf01−Prf03, Prf07, and Prf08 is biased toward an acidic pH region, suggesting that some acidic residues in a stem-forming region or its vicinity contribute to this process. A probable candidate for this is the FVHDCV sequence (residues 175−180), in which the Asp residue appears to confer such a pH dependency. Although these peptides show evidence of amyloidogenicity at an acidic pH, their stem-forming region is likely to differ from those of the peptides that form amyloids at a physiological pH.

The amyloidogenic peptides found in this study and their related peptides including no-amyloid peptides are summarized in Figure 6. These peptides can be classified into three categories: groups 1−3. The peptides in groups 1 and 2 include eight or more residues from among the 10 residues of peptides 180−184 and 189−193, which were selected as described below. Groups 1 and 2 involve amyloidogenic and non-amyloidogenic peptides, respectively. The peptides in group 3 are amyloidogenic but not sufficiently so to fulfill the above numeric condition. These two sequence regions (residues 180−184 and 189−193) are characteristically rich in hydrophobic residues as well as in β-branched residues, which are favorable for the stabilization of the β-structure. With regard to groups 1 and 2, among the 13 peptides containing VTTTT as residues 189−193, the occurrence fractions of amyloidogenic peptides were determined to be 0.71 (=5/7) for DCVNI (residues 178−182) ("5/7" means five amyloidogenic peptides found among seven examined peptides containing DCVNI), 0.78 (=7/9) for CVNIT (residues 179−183), 0.80 (=8/10) for VNITI

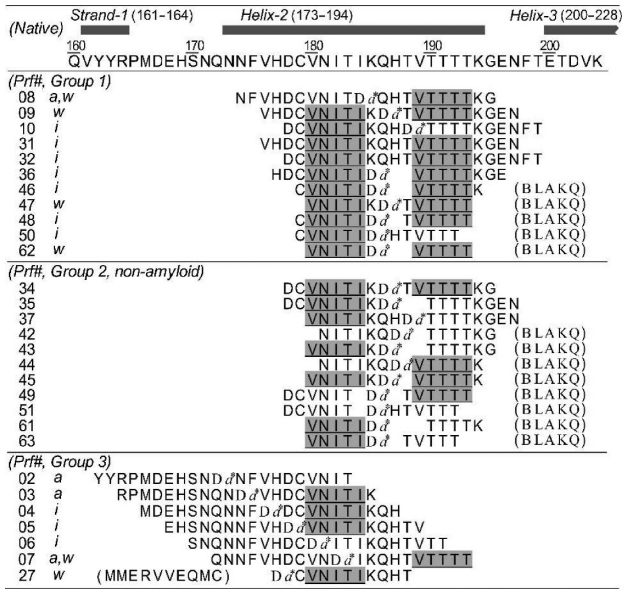

Figure 6. Comparison of the sequences for amyloidogenic peptides and no-amyloidogenic ones but with sequence similarity for the former. The peptides in groups 1 and 2 contain eight or more native residues among 10 residues of peptides 180−184 and 189−193. Group 3 is for the peptides below this criteria. Amyloidogenic peptides are shown in groups 1 and 3. The amyloid forming properties detected by the ThT binding assay are typically indicated with i, w, and a for the cases of intensive fluorescence, weak fluorescence, and fluorescence only at acidic pH, respectively. The secondary structures of the native prion protein taken from the structural information (PDB entry 1QLX) are shown above the sequences. Special amino acid codes *a** and B denote L-Ala and β-Ala, respectively.

(residues 180−184), and 0.57 (=4/7) for NITIK (residues 181−185). Thus, the VNITI sequence indicates the highest percentage among these. On the other hand, among 17 types of peptides bearing the VNITI sequence at positions 180−184, the occurrence fractions of amyloidogenic peptides were 0.75 (=6/8) for TVTTT (residues 188−192), 0.80 (=8/10) for VTTTT (residues 189−193), and 0.50 (=6/12) for TTTTK (residues 190−194). Therefore, the combination of VNITI (residues 180−184) and VTTTT (residues 189−193) appears to be the most preferable pairing for inducing amyloidogenicity. As a fundamental structural model for amyloids, it is likely that these two strands constitute stem-forming regions that form an intramolecular β-sheet structure stabilized by interstrand hydrogen bonds.

Focusing on the pair of VNITI (residues 180−184) and VTTTT (residues 189−193) sequences, the absence of Val180 leads to the disappearance of amyloidogenicity, as seen for Prf42 and Prf44. Similarly, the absence of Ile184 results in a decrease in amyloidogenicity, resulting in no amyloidogenicity for Prf49 and Prf51, and a lowered amyloidogenicity for Prf08. Most remarkably, the peptides lacking Val189, such as Prf35, Prf37, Prf42, Prf43, and Prf61, completely lose their amyloid forming properties. These results suggest that hydrophobic interactions between side chains such as Ile184 and Val189, located on the different β-strands but spatially in contact with each other, are crucial for amyloid formation. This is in line with the fundamental structural model proposed for the amyloid derived from the barnase fragment.[23] In addition, the absence of Thr193 for Prf50 leads to a low F_P/F_{500} value for the ThT-bound form (Figure 5), indicating the necessity of Thr193

dx.doi.org/10.1021/bi201688r | Biochemistry 2012, 51, 1566−1576

for the formation of an amyloid structure of the native sequence.

Generally, when a compact type II turn accompanied by an intramolecular β-sheet structure is formed, as in the case of two β-strands linked by the Asp-Ala* pair, the two residues next to Asp and Ala* of this linkage form an intramolecular hydrogen bond, according to the stereochemical constraints. The intramolecular hydrogen bonds alternate along the sequences of β-strands in an antiparallel orientation. In fact, peptides including VNITI-D*a**-VTTTT, such as Prf36, Prf46, and Prf62, where D*a** denotes the Asp-Ala* pair, exhibited amyloidogenicity. In particular, Prf36 and Prf46 showed a substantial propensity to form amyloids. This can be attributed to the stabilization by hydrogen bonding between Ile184 and Val189 in addition to the hydrophobic interactions between their side chains. In contrast, peptides including VNITI-K-D*a**-T-VTTTT, such as Prf09, Prf47, and Prf34, showed relatively low or no amyloidogenicity. In the latter case, Ile184 and Val189 cannot bond because of the outward orientation of the C═O and N−H groups in these residues, although hydrophobic interactions seem possible in the form of a β-sheet. This indicates that not only a pairing of hydrophobic residues but also their positions in relation to the alternate hydrogen bonding pattern along the β-strands may be critical factors in the stabilization of an intramolecular β-sheet, which would lead to amyloid structures.

The amyloid-forming peptides listed in group 3 significantly lack either VNITI (residues 180−184) or VTTTT (residues 189−193). As estimated from the areas of the major peaks, the amyloid-forming Prf04 in group 3 has a fairly low β-structure content (49% area) in comparison with Prf10 (60% area) and Prf36 (66% area) in group 1 (Figure 3). This suggests that the amyloid derived from Prf04 is constructed of a single β-strand in a respective molecule. In contrast, Prf36, showing a high β-structure content, is likely to form amyloids with a pair of β-strands in the molecule, as discussed above for the peptides in group 1. On the basis of the similarity in CD spectra for Prf04−Prf06 (Figure 2), these peptides are thought to form amyloid structures in a manner analogous to that of a "single β-strand". Electron microscopy observations of Prf04 and Prf10 also suggest differences in the amyloid structures of these peptides belonging to groups 3 and 1, respectively (Figure 4). Thus, most of the peptides in group 3 appear to form amyloids via the integration of single β-strands around a neutral pH, because they lack either one of a pair of stem-forming regions, in addition to containing no other hydrophobic region.

The results are summarized as follows. Two strands of VNITI (residues 180−184) and VTTTT (residues 189−193), namely, $\beta_{am}1$ and $\beta_{am}2$, respectively, are most likely to form an intramolecular β-sheet structure, accompanied by their hydrophilic linkage KQHT (residues 185−188) as a loop region. This pair of β-strands would be stem-forming regions for full-length prion proteins as a framework of amyloids. Among the 10 residues of probable β-strands, no fewer than nine are β-branched amino acids, which play an important role in the stabilization of the β-structure. Moreover, hydrophobic interactions between Ile184 and Val189 clearly could contribute definitively to the joining up of potential stem-forming regions.

These two stem-forming regions, peptides 180−184 and 189−193, coincide well with two of the four highly ordered regions estimated by the Monte Carlo−simulated annealing algorithm for solid-state NMR data of Syrian hamster PrP, i.e., residues 181−185, 189−193, 199−203, and 221−225, of which the residue numbers were read out from the figure in the literature.[21] In a review of our data on the basis of the four regions named here, namely, $\beta_{am}1$−$\beta_{am}4$, respectively, the peptides containing only one region among $\beta_{am}2$−$\beta_{am}4$, which are {Prf07, 08, 15; 12, 18, 19, 20; 23, and 24}, showed no amyloidogenicity. With regard to the pairing of two neighboring β_{am} strands, peptides such as Prf13 and Prf14 containing both $\beta_{am}2$ and $\beta_{am}3$ show no indication of amyloidogenicity, in contrast with peptides such as Prf10 composed of the $\beta_{am}1$ and $\beta_{am}2$ pair. The $\beta_{am}3$ and $\beta_{am}4$ strands are located some distance from each other, so that the pairing of these two β-strands would be a rare event. In summary, the $\beta_{am}1$ and $\beta_{am}2$ pair is most likely to be a primary stem-forming region, and the regions containing $\beta_{am}3$ and $\beta_{am}4$ may secondarily participate in amyloid core formation.

Structural Transition of Stem-Forming Regions. The experimentally identified stem-forming regions, peptides 180−184 and 189−193, were mapped on the structure of a prion protein in the soluble monomeric state (Figure 7A). The region

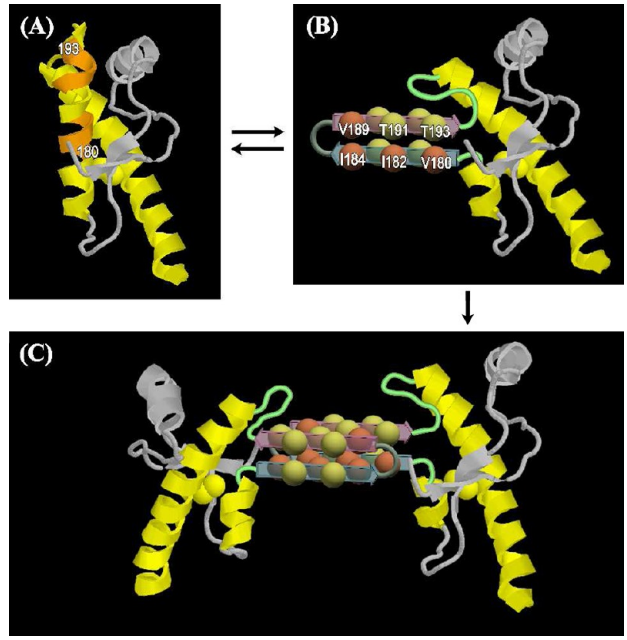

Figure 7. Proposed structural transition of prion protein on the basis of the identified stem-forming regions. (A) The native structure in a monomer state is illustrated for residues 125−228 with the data of PDB entry 1QLX. The identified stem-forming regions, residues 180−184 and 189−193, are mapped on the ternary structure. (B) The transient conformation was assumed as a locally transformed one with an exposed intramolecular β-sheet consisting of the stem-forming regions. The structure of the region except residues 180−199 was drawn like a native one, for the sake of convenience. (C) The probable dimer of prion would be formed by the interaction between hydrophobic faces of the exposed intramolecular β-sheets. Two monomers in this form are expected to adopt *C*2 symmetry for the direction along the hydrogen bonding in the β-sheets. In this figure, the conformation of the H3 region remains in the α-helix form as in a monomer state, because no detailed data about the conformation of this region in the associated states are available, although recent solid-state NMR studies revealed that the core domain corresponding to the H2−H3 region mainly consists of β-structure rather than α-helix.[21]

of residues 180−193 covering these two regions corresponds to approximately two-thirds of α-helix H2 (residues 173−194), which interacts with the N-terminal half of α-helix H3 (residues

dx.doi.org/10.1021/bi201688r | *Biochemistry* 2012, 51, 1566−1576

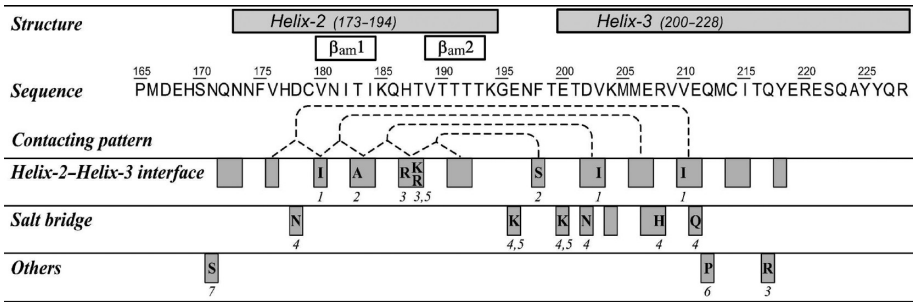

Figure 8. Locations of the causative mutations for prion diseases and the potential stem-forming regions. The secondary structures are taken from the data of PDB entry 1QLX for a monomeric prion. Experimentally identified stem-forming regions are indicated as strands $\beta_{am}1$ and $\beta_{am}2$. The spatial relation of the interacting α-helices, helix 2 and helix 3, is shown as a contacting pattern with dashed lines. The residues located at the helix 2–helix 3 interface and those bearing salt bridge interactions are indicated with rectangular blocks in the bottom half of this figure. The causative mutations are exhibited with amino acid codes on them accompanied by numeric codes for detailed descriptions for the reasons of destabilization. The related numeric codes are as follows: *1*, expanding the distance between two helices; *2*, forming a cavity at the interface of the helices; *3*, emerging charges inside the protein; *4*, vanishing salt bridge interaction; *5*, causing charge repulsion; *6*, breaking the continuity of an α-helix; *7*, undefined.

200–228) to form the native folded structure. Because of a disulfide linkage between Cys179 and Cys214, these helices are joined together. A probable model for the transient β-sheet structure of stem-forming regions is indicated in Figure 7B, where, for the sake of convenience, the native structure is adopted for regions other than the stem-forming regions and their neighboring loops. Interestingly, it has been reported that a prion protein involves the formation of a metastable conformer (PrP*) in a small percentage of molecules associated with the disordered structure of the region of H2 and H3.[33] This is consistent with our estimation of the locations of the stem-forming regions. Therefore, it would be fairly valid to conclude that these stem-forming regions undergo a transition from an α-helix to a β-structure as formed in amyloids through a locally unfolded conformational state between the structures shown in panels A and B of Figure 7.

In this β-sheet structure, highly hydrophobic residues, Val180, Ile182, Ile184, and Val189, are present on identical surfaces of the β-sheet (Figure 7B). Therefore, stacked β-sheets can be proposed as the dimer structure of a prion protein, which is known to be formed in cases where a locally unfolded structure is induced by treatment with 0.2% SDS[13] (Figure 7C). This dimer would be stabilized by the interaction between the hydrophobic surfaces of β-sheets. It should be noted that the structure shown in Figure 7B, which is herein termed an exposed β2-structure, appears to be naturally metastable and probably transient but that its form is highly effective for further molecular integration.

Because the probability of an exposed β2-structure is thought to be very low, like that of PrP*, an encounter between two exposed β2-structures would be a negligibly rare event. Consequently, this leads to the absence of an initiation reaction for amyloid formation. This may be the reason why a normal prion protein itself never causes a prion disease in vivo. The formation of amyloid from prion proteins would be possible only by the adhesion of the exposed β2-structure onto preformed amyloids such as extraneous prions with infectivity. Meanwhile, amyloids of prion proteins so far have been prepared by treatment with SDS or urea.[12−16] Under in vitro conditions, relatively mild denaturation agents may enhance the content of exposed β2-structure, which would be favorable for enhancing amyloid formation.

Using solid-state NMR to investigate amyloids of PrP containing ^{13}C-labeled phenylalanines or isoleucines, Tycko et al. proposed the formation of an in-register parallel β-sheet structure for amyloid fibrils based on the pattern of isotope nuclei for labeling.[21] Although we have no direct data related to a higher-order structure of amyloids, the stable formation of a (β-strand)-loop-(β-strand) structure with intramolecular hydrogen bonds appears to lead to in-register parallel arrangements of β2-structure units in fibrils, which corresponds to a form constructed by the translational arrangement of the dimer shown in Figure 7C. In spite of the difference in the type of β-sheet between Tycko's model and ours, the model described here can explain the vicinity of specific amino acid residues such as ^{13}C-labeled phenylalanines in fibrils.

Recently, it was revealed that the fragment corresponding to the H2–H3 domain, residues 167–234 for ovine PrP, takes nativelike folded structure and undergoes amyloid formation in a manner similar to that of the full-length prion protein.[34] Also, the patterns of oligomeric species are comparable for the fragment and full-length PrP.[35] The H2–H3 domain is most likely to play an important role in seeding for amyloid growth.[8] These results favorably support the significance of the stem-forming region identified in this work. The molecular dynamics study detected a conformationally stable β-sheet structure in the early stage of oligomerization.[35] It was reported that the first hairpin is V183–I191/I208–M216 and the second V192–T196/Q199–Q203. The first β-strands of these two hairpins correspond to V180–T188 and V189–T193 of human PrP. These two β-strands coincide well with our stem-forming regions.

As a specific structure, a swapped dimer was revealed for reduced PrP by X-ray crystal analysis.[36] In the structure denoted as PDB entry 3HJ5, the region of residues 191–193 forms an antiparallel β-sheet structure intermolecularly. Although this structure is different from our model shown in Figure 7C because of the lack of a disulfide linkage, the intermolecular β-sheet formation of residues 191–193 suggests some propensity for β-structure formation in the region of VTTTT (residues 189–193). In addition, a monoclonal antibody for the sequence YY (residues 162 and 163) was developed to recognize scrapie PrP but not normal PrP.[37] This region is in the relative proximity of one of the stem-forming regions, VNITI (residues 180–184), in a monomer state, so

dx.doi.org/10.1021/bi201688r | *Biochemistry* 2012, 51, 1566–1576

that the specificity of this antibody is likely to be associated with the structural transition of peptide 180−184, thus affecting the probable exposure of YY (residues 162 and 163). Thus, our model is compatible with the other experimental results.

Promotion of Exposed β2-Structure by Causative Mutations. Various causative mutations have been reported for the inherited prion diseases in the regions of residues 102−131 and 171−217, as in a list with the ID code of PRIO_HUMAN in the UniProt database (see Table S3 of the Supporting Information). The latter region involves potential stem-forming regions described in this work and lies on the H2−H3 domain. The mutations are indicated in the bottom half of Figure 8. The steric relationship of α-helices H2 and H3 is also expressed in the "Contacting pattern" section. These helices interact with each other basically in a ridge-in-groove manner; for example, Val210 is located between Val176 and Val180 (see the dashed line in Figure 8). The residues located at the interface of H2 and H3 are represented by gray rectangles along the sequence, and the causative mutations in these positions are shown for them with amino acid codes.

Mutations V180I, T183A, H187R, T188K, and T188R are involved in the region of stem-forming ones and the intervening loop. These mutations have disadvantages for stabilization at the interface of H2 and H3 for the reason shown with numeric codes in Figure 8. However, these mutations seem to have no disadvantage for the stabilization of a stem-forming β-sheet and indeed are expected to stabilize it. Interestingly, mutations F198S, D202N, V203I, V210I, and E211Q are located in the region of helix H3 facing helix H2 containing stem-forming regions. These mutations also appear to destabilize the helix structures of H2 and H3. Destabilizations by these mutations at the H2−H3 interface can be attributed to "extensional mutations", "cavity-forming mutations", and "mutations inducing inner charge". Mutations T188K and T188R lead to unfavorable electrostatic repulsion between the helices against Lys185. It should be noted that all of these causative mutations are involved in the sequence of the stem-forming domain (residues 180−193) and its counterpart (residues 198−211) in a native monomer structure. Although positions 173, 176, 214, and 218 constitute the H2−H3 interface, no causative mutations have been found.

The residues that participate in salt bridge interactions and contribute to the stabilization of the native structure are also shown in Figure 8 (see the "Salt bridge" section). Six causative mutations, D178N, E196K, E200K, D202N, R208H, and E211Q, can be detected on the salt-bridging residues. All of these mutations result in a loss of native salt bridges, and some result in charge repulsion. Therefore, the causative mutations relevant to salt bridges are likely to destabilize the native structure of the H2−H3 domain. The regions of causative mutations for the H2−H3 interface and those for the salt bridge are well superimposed, suggesting that these mutations destabilize the region sandwiched by Cys179 and Cys214 to allow the exposure of stem-forming regions. Consequently, most causative mutations would enhance the relative stability of the exposed β2 structure, as shown in Figure 7B. This rationally explains why prions with causative mutations undergo amyloid formation without extraneous structural cores.

Volume Effect Estimated for Amyloid Formation. In this work, the authors propose an "exposed β2-driven mechanism" for amyloid formation on the basis of the identified stem-forming regions. This model involves the integration of prion molecules with a small stem domain (14 residues) and a large nonstem domain (194 residues). The proposed structures for the amyloids are illustrated in Figure 9.

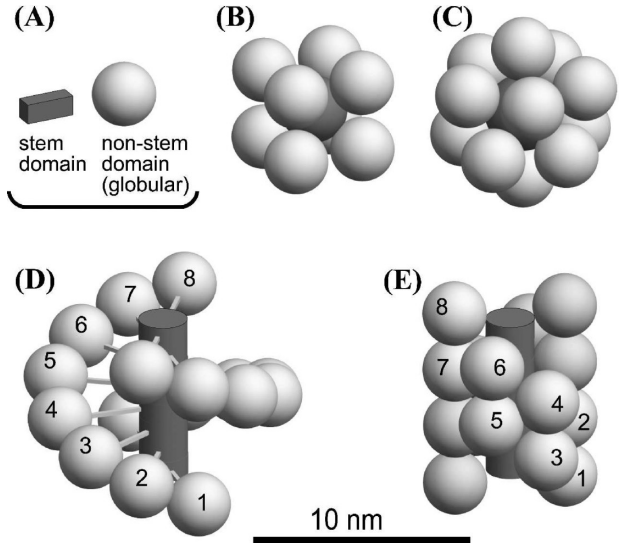

Figure 9. Perspective consideration of the associated structures of prion proteins involving volume effects. (A) The stem domain (residues 180−193) forming an intramolecular β-sheet and the nonstem domain as a globular part with 100 residues are illustrated with volume models. For an actual prion protein, a peptide chain of ~100 residues with a random-coil structure sprawls from this globular domain. The volume is calculated on the basis of the averaged volume of amino acid residues in globular proteins, 0.135 nm^3 per a residue, which is derived from specific partial volumes. (B) Model of the octamer. The stem domains are integrated into a sphere with an equal volume surrounded by eight nonstem domains, which are in close contact with the stem domain. (C) Model for a 12-mer of a prion protein with the symmetry of a regular dodecahedron. The nonstem domains have no contact with each other. (D) Model of a fibril illustrated for a partial structure of 16-mer forming two-sheet cross-β-structure. The stem domains are integrated into a cylinder without changing the volume or axial length. The nonstem domain is connected with the stem domain by a 2.5 nm linker as an example. The neighboring nonstem domains just contact each other. (E) Fibril model with a zigzag arrangement of nonstem domains different from the former. A nonstem domain directly contacts four neighboring ones, and the stem domain is depicted as a cylinder.

A globular rigid body with only 100 residues for the sake of convenience is shown as a nonstem domain because the remaining N-terminal region, with ~100 residues, seems disordered and is free to form any shape. Assuming steric regularity in the form of amyloid fibrils, both an impermissibly long radial linker and an extremely twisted arrangement of nonstem domains are necessary (Figure 9D). Otherwise, a zigzag arrangement may loosen the twisting stress to some extent (Figure 9E). In any case, nonstem domains in prion fibrils should be subjected to a severely crowded situation or deformation from their native forms. This may be the reason polymorphism is observed for fibrils prepared under different conditions.[19,38]

In contrast with the fibrils, oligomers with spherical symmetry are thought to be facile, because of their liberation from conflicts between nonstem domains (Figure 9B,C). Oligomers with specific numbers of monomers, such as 8-mers or 12(−14)-mers, have been reported.[12,15,16] Compared with oligomer formation, fibril growth might entail further difficulties in the incorporation of a monomer because of the

hindrance by a large nonstem domain at the elongating terminus. For the same reason, growth of amyloid from an oligomer such as an octamer also would be expected to be hindered. In fact, it was reported that the fibril of mouse PrP is not the product of a stable oligomer.[12]

The 22-residue peptide Prf32 (residues 178−199) forms relatively uniform amyloid fibrils, as shown in Figure 4D but without the particle-shaped association species. The fragment peptide of ovine PrP with 62 residues of peptide 168−229 is known to form oligomers as well as amyloid fibrils.[8] Interestingly, under the condition where mouse PrP(90−230) with 141 residues forms the fibrils, mouse PrP(23−230), with 208 residues, forms only particle-shaped associated species.[39] Thus, in spite of the fact that the same stem-forming regions are present in these peptides and proteins, the associated forms are different. Small amyloidogenic peptides within 20 residues generally form only fibrils.[24] When these observations are taken into account, the formation of particle-shaped aggregates or oligomers would be closely related to the volume effect of the nonstem domains.

Comparison of Species from Different Organisms. The stem-forming regions for human PrP, VNITI (residues 180−184) and VTTTT (residues 189−193), are identical to those of mouse, hamster, and rat. In the corresponding region, the PrP of bovine, horse, sheep, pig, and rabbit has only an I184V mutation (this residue number is for humans). Additionally, the loop region, KQHT (residues 185−188), is identical among these organisms except for the Q186E mutation in the bovine form. This sequence homology suggests that the structures of the stem domains for these mammalian molecules are similar. However, even for closely related animals, such as the mouse and hamster, which contain quite identical sequences in peptide 171−202, a species barrier exists for an infection of a prion disease. The only way to explain this species barrier is that the interaction between nonstem domains is a determinant of this phenomenon. The difference in the lateral assembly of amyloid fibrils from the mouse and hamster[40] is consistent with this consideration.

The prion proteins of avians, reptiles, and amphibians have a similar structure in the monomer state.[2] The sequences for peptides 180−193 corresponding to the stem-forming regions of the human are FNITV-xxxx-IGPAA for chicken, VNITV-xxxx-IDPKE for turtle, and FNMSV-xxxx-IKPAE for *Xenopus*, where xxxx denotes a respective loop region (see the sequence alignment in Figure S4 of the Supporting Information). Thus, similarities exist between the first strands with the sequence for the human, VNITI. However, the second strands are quite different from that of human, VTTTT. The presence of Pro191 in addition to hydrophilic residues in this strand would be a critical defect for the conversion into a β-structure of an amyloid. This clearly explains why no animals other than mammals suffer from prion diseases.

CONCLUSION

On the basis of the experimental identification of stem-forming regions as a core of amyloids, we propose that prion proteins form amyloids according to an exposed β2-driven mechanism, which involves an intramolecular β-sheet derived from potential stem-forming regions by local transformation. This mechanism provides a valid explanation for why normal prion proteins do not form amyloids without importing the infectious source and why some mutations in a specific region are determinants of pathogenicity. We also successfully elucidated the mechanism involved in the regulation of the shapes of amyloids, i.e., fibrils, particles, or oligomers, by using the volume effect of nonstem domains, which is actualized for large proteins. The identification of stem-forming regions and the exposed β2-driven mechanism should help significantly in the elucidation of infectivity and pathogenicity as well as in the development of methods designed to suppress prion-related diseases.

ASSOCIATED CONTENT

Supporting Information

Numerical values concerning the fluorescence spectra of ThT in the presence of incubated Prf peptides and classification of amyloidogenicity (Table S1), parameters for Gaussian curves obtained by component resolving analysis of IR spectra represented in Figure 3 and Figure S3 along with assignment of absorption bands to the structures (Table S2), a list of pathogenic mutations for the human prion protein (Table S3), correlation between fluorescence enhancement of ThT and molar ellipticity for the incubated Prf peptides (Figure S1), correlation between fluorescence enhancement of ThT and the spectral parameter, F_P/F_{500}, reflecting a shift in the maximal fluorescence wavelength (Figure S2), IR spectra of the amyloids from the Prf peptides (Figure S3), and sequence alignment of the prion proteins from the various vertebrates (Figure S4). This material is available free of charge via the Internet at http://pubs.acs.org.

AUTHOR INFORMATION

Corresponding Author

*Central 6, 1-1-1 Higashi, Tsukuba, Ibaraki 305-8566, Japan. Phone: +81-29-861-9466. Fax: +81-29-836-5807. E-mail: morii.hi@aist.go.jp.

Present Address

[⊥]Tokyo University of Science, Yamaguchi, Japan,

Notes

The authors declare no competing financial interest.

ABBREVIATIONS

PrP, prion protein; CJD, Creutzfeldt-Jakob disease; GSD, Gerstmann-Straussler disease; H−D, hydrogen−deuterium; SDS, sodium dodecyl sulfate; H2, second helix in the structure of monomeric PrP, also indicated as helix 2 (H3 is similarly defined); β_{am}, β-strand in the core of amyloids (the accompanying numeric character is given in order from the N-terminus, e.g., β_{am}2); ThT, thioflavin T; Prf, name of a series of synthetic peptides examined in this work; D*a**, (D-Asp)-(L-Ala), also indicated as Asp-Ala*; β-Ala, 3-aminopropionic acid; PDB, Protein Data Bank.

REFERENCES

(1) Riek, R., Hornemann, S., Wider, G., Billeter, M., Glockshuber, R., and Wüthrich, K. (1996) NMR structure of the mouse prion protein domain PrP(121−231). *Nature 382*, 180−182.

(2) Calzolai, L., Lysek, D. A., Pérez, D. R., Güntert, P., and Wüthrich, K. (2005) Prion protein NMR structures of chickens, turtles, and frogs. *Proc. Natl. Acad. Sci. U.S.A. 102*, 651−655.

(3) Prusiner, S. B., McKinley, M. P., Bowman, K. A., Bolton, D. C., Bendheim, P. E., Groth, D. F., and Glenner, G. G. (1983) Scrapie prions aggregate to form amyloid-like birefringent rods. *Cell 35*, 349−358.

(4) Safar, J., Roller, P. P., Gajdusek, D. C., and Gibbs, C. J. Jr. (1993) Conformational transitions, dissociation, and unfolding of scrapie amyloid (prion) protein. *J. Biol. Chem. 268*, 20276−20284.

(5) Silveira, J. R., Raymond, G. J., Hughson, A. G., Race, R. E., Sim, V. L., and Caughey, B. (2005) The most infectious prion protein particles. *Nature 437*, 257−261.
(6) Prusiner, S. B., Groth, D. F., Bolton, D. C., Kent, S. B., and Hood, L. E. (1984) Purification and structural studies of a major scrapie prion protein. *Cell 38*, 127−134.
(7) Bocharova, O. V., Breydo, L., Parfenov, A. S., Salnikov, V. V., and Baskakov, I. V. (2005) In vitro conversion of full-length mammalian prion protein produces amyloid form with physical properties of PrP^{Sc}. *J. Mol. Biol. 346*, 645−659.
(8) Adrover, M., Pauwels, K., Prigent, S., de Chiara, C., Xu, Z., Chapuis, C., Pastore, A., and Rezaei, H. (2010) Prion fibrillization is mediated by a native structural element that comprises helices H2 and H3. *J. Biol. Chem. 285*, 21004−21012.
(9) Kaneko, K., Ball, H. L., Willie, H., Zhang, H., Groth, D., Torchia, M., Tremblay, P., Safar, J., Prusiner, S. B., DeArmond, S. J., Baldwin, M. A., and Cohen, F. E. (2000) A synthetic peptide initiates Gerstmann-Sträussler-Scheinker (GSS) disease in transgenic mice. *J. Mol. Biol. 295*, 997−1007.
(10) Gasset, M., Baldwin, M. A., Lloyd, D. H., Gabriel, J.-M., Holtzman, D. M., Cohen, F., Fletterick, R., and Prusiner, S. B. (1992) Predicted α-helical regions of the prion protein when synthesized as peptides form amyloid. *Proc. Natl. Acad. Sci. U.S.A. 89*, 10940−10944.
(11) Tagliavini, F., Prelli, F., Verga, L., Giaccone, G., Sarma, R., Gorevic, P., Ghetti, B., Passerini, F., Ghibaudi, E., Forloni, G., Salmona, M., Bugiani, O., and Frangione, B. (1993) Synthetic peptides homologous to prion protein residues 106−147 form amyloid-like fibrils in vitro. *Proc. Natl. Acad. Sci. U.S.A. 90*, 9678−9682.
(12) Baskakov, I. V., Legname, G., Baldwin, M. A., Prusiner, S. B., and Cohen, F. E. (2002) Pathway complexity of prion protein assembly into amyloid. *J. Biol. Chem. 277*, 21140−21148.
(13) Post, K., Pitschke, M., Schäfer, O., Wille, H., Appel, T. R., Kirsch, D., Mehlhorn, I., Serban, H., Prusiner, S. B., and Riesner, D. (1998) Rapid acquisition of β-sheet structure in the prion protein prior to multimer formation. *Biol. Chem. 379*, 1307−1317.
(14) Stöhr, J., Weinmann, N., Wille, H., Kaimann, T., Nagel-Steger, L., Birkmann, E., Panza, G., Prusiner, S. B., Eigen, M., and Riesner, D. (2008) Mechanisms of prion protein assembly into amyloid. *Proc. Natl. Acad. Sci. U.S.A. 105*, 2409−2414.
(15) Leffers, K.-W., Schell, J., Jansen, K., Lucassen, R., Kaimann, T., Nagel-Steger, L., Tatzelt, J., and Riesner, D. (2004) The structural transition of the prion protein into its pathogenic conformation is induced by unmasking hydrophobic sites. *J. Mol. Biol. 344*, 839−853.
(16) Gerber, R., Tahiri-Alaoui, A., Hore, P. J., and James, W. (2007) Oligomerization of the human prion protein proceeds via a molten globule intermediate. *J. Biol. Chem. 282*, 6300−6307.
(17) Tahiri-Alaoui, A., Sim, V. L., Caughey, B., and James, W. (2006) Molecular heterosis of prion protein β-oligomers. *J. Biol. Chem. 281*, 34171−34178.
(18) Lu, X., Wintrode, P. L., and Surewicz, W. K. (2007) β-sheet core of human prion protein amyloid fibrils as determined by hydrogen/deuterium exchange. *Proc. Natl. Acad. Sci. U.S.A. 104*, 1510−1515.
(19) Smirnovas, V., Kim, J.-I., Lu, X., Atarashi, R., Caughey, B., and Surewicz, W. K. (2009) Distinct structures of scrapie prion protein (PrP^{Sc})-seeded versus spontaneous recombinant prion protein fibrils revealed by hydrogen/deuterium exchange. *J. Biol. Chem. 284*, 24233−24241.
(20) Cobb, N. J., Sönnichsen, F. D., McHaourab, H., and Surewicz, W. K. (2007) Molecular architecture of human prion protein amyloid: A parallel, in-register β-structure. *Proc. Natl. Acad. Sci. U.S.A. 104*, 18946−18951.
(21) Tycko, R., Savtchenko, R., Ostapchenko, V. G., Makarava, N., and Baskakov, I. V. (2010) The α-helical *C*-terminal domain of full-length recombinant PrP converts to an in-register parallel β-sheet structure in PrP fibrils. *Biochemistry 49*, 9488−9497.
(22) Kuwata, K., Kamatari, Y., Akasaka, K., and James, T. L. (2004) Slow conformational dynamics in the hamster prion protein. *Biochemistry 43*, 4439−4446.
(23) Saiki, M., Honda, S., Kawasaki, K., Zhou, D., Kaito, A., Konakahara, T., and Morii, H. (2005) Higher-order molecular packing in amyloid-like fibrils constructed with linear arrangements of hydrophobic and hydrogen-bonding side-chains. *J. Mol. Biol. 348*, 983−998.
(24) Saiki, M., Konakahara, T., and Morii, H. (2006) Interaction-based evaluation of the propensity for amyloid formation with cross-β structure. *Biochem. Biophys. Res. Commun. 343*, 1262−1271.
(25) Morii, H., Saiki, M., Konakahara, T., and Ishimura, M. (2006) Peripheral region for core cross-β plays important role in amyloidogenicity. *Biochem. Biophys. Res. Commun. 342*, 808−816.
(26) Morii, H., Takenawa, T., Arisaka, F., and Shimizu, T. (1997) Identification of kinesin neck region as a stable α-helical coiled coil and its thermodynamic characterization. *Biochemistry 36*, 1933−1942.
(27) Sohma, Y., Chiyomori, Y., Kimura, M., Fukao, F., Taniguchi, A., Hayashi, Y., Kimura, T., and Kiso, Y. (2005) *O*-Acyl isopeptide method for the efficient preparation of amyloid β peptide 1−42 mutants. *Bioorg. Med. Chem. 13*, 6167−6174.
(28) Wadai, H., Yamaguchi, K., Takahashi, S., Kanno, T., Kawai, T., Naiki, H., and Goto, Y. (2005) Stereospecific amyloid-like fibril formation by a peptide fragment of β2-microglobulin. *Biochemistry 44*, 157−164.
(29) Nara, M., Morii, H., Yumoto, F., Kagi, H., and Tanokura, M. (2006) Fourier transform infrared spectroscopic study on the Ca^{2+}-bound coordination structures of synthetic peptide analogues of the calcium-binding site III of troponin C. *Biopolymers 82*, 339−343.
(30) Hutchinson, E. G., and Thornton, J. M. (1994) PROMOTIF: A program to identify and analyze structural motifs in proteins. *Protein Sci. 3*, 2207−2216.
(31) Miyazawa, T., and Blout, E. R. (1961) The infrared spectra of polypeptides in various conformations: Amide I and II bands. *J. Am. Chem. Soc. 83*, 712−719.
(32) Zandomeneghi, G., Krebs, M. R. K., McCammon, M. G., and Fändrich, M. (2004) FTIR reveals structural differences between native β-sheet proteins and amyloid fibrils. *Protein Sci. 13*, 3314−3321.
(33) Kuwata, K., Li, H., Yamada, H., Legname, G., Prusiner, S. B., Akasaka, K., and James, T. L. (2002) Locally disordered conformer of the hamster prion protein: A crucial intermediate to PrP^{Sc}? *Biochemistry 41*, 12277−12283.
(34) Xu, Z., Prigent, S., Deslys, J.-P., and Rezaei, H. (2011) Dual conformation of H2H3 domain of prion protein in mammalian cells. *J. Biol. Chem. 286*, 40060−40068.
(35) Chakroun, N., Prigent, S., Dreiss, C. A., Noinville, S., Chapuis, C., Fraternali, F., and Rezaei, H. (2010) The oligomerization properties of prion protein are restricted to the H2H3 domain. *FASEB J. 24*, 3222−3231.
(36) Knaus, K. J., Morillas, M., Swietnicki, W., Malone, M., Surewicz, W. K., and Yee, V. C. (2001) Crystal structure of the human prion protein reveals a mechanism for oligomerization. *Nat. Struct. Biol. 8*, 770−774.
(37) Paramithiotis, E., Pinard, M., Lawton, T., LaBoissiere, S., Leathers, V. L., Zou, W.-Q., Estey, L. A., Lamontagne, J., Lehto, M. T., Kondejewski, L. H., Francoeur, G. P., Papadopoulos, M., Haghighat, A., Spatz, S. J., Head, M., Will, R., Ironside, J., O'Rourke, K., Tonelli, Q., Ledebur, H. C., Chakrabartty, A., and Cashman, N. R. (2003) A prion protein epitope selective for the pathologically misfolded conformation. *Nat. Med. 9*, 893−899.
(38) Cobb, N. J., Apetri, A. C., and Surewicz, W. K. (2008) Prion protein amyloid formation under native-like conditions involves refolding of the C-terminal α-helical domain. *J. Biol. Chem. 283*, 34704−34711.
(39) El Moustaine, D. E., Perrier, V., Smeller, L., Lange, R., and Torrent, J. (2008) Full-length prion protein aggregates to amyloid fibrils and spherical particles by distinct pathways. *FEBS J. 275*, 2021−2031.
(40) Makarava, N., Bocharova, O. V., Salnikov, V. V., Breydo, L., Anderson, M., and Baskakov, I. V. (2006) Dichotomous versus palm-type mechanisms of lateral assembly of amyloid fibrils. *Protein Sci. 15*, 1334−1341.